

# Phase Separation in Binary and Ternary Polymer Composites Studied with Electronic Excitation Transport

Deborah M. Hussey<sup>†</sup> and M. D. Fayer<sup>\*</sup>

Department of Chemistry, Stanford University, Stanford, California 94305-5080

Received March 19, 1999; Revised Manuscript Received July 16, 1999

**ABSTRACT:** Time-resolved fluorescence polarization anisotropy decay measurements are used to observe the process of phase separation of molecularly mixed polymer blends. The binary blends are composed of a low concentration of poly[methyl methacrylate-*co*-2-vinylnaphthalene] (PMMA2VN) in poly[vinyl acetate] (PVAc). The small number of 2VN groups on the PMMA2VN chains act as fluorescent chromophores. Electronic excitation transport (EET) among these chromophores contributes to the decay of their fluorescence polarization anisotropy, which is measured with time-correlated single photon counting. Since EET is highly sensitive to the distances between chromophores, it reflects their spatial distribution and can reveal both the isolated-chain structure and the aggregation of polymer chains in the blend on the nanometer distance scale. Blend samples are prepared by annealing a homogeneous blend at an elevated temperature for a given time and then rapidly quenching the phase-separating material below its glass-transition temperature. The newly formed nanoscopic aggregates frozen in the sample are then investigated with EET. The ternary blends are composed of a very small amount of PMMA2VN and a larger quantity of PMMA, both in bulk PVAc. In the phase separation of ternary blends, the PMMA2VN component initially partitions with its chromophore-free counterpart, expanding to its  $\theta$ -condition size before continuing to aggregate and eventually separating from the PMMA.

## I. Introduction

The desire to create materials that are tailored for particular applications in an inexpensive, environmentally sensible manner has made the prediction of the physical properties of polymer blends from those of their components one of the important challenges of modern materials science. A difficulty with making blends is that few polymers are completely miscible or compatible over a wide range of temperatures, pressures, and compositions,<sup>1</sup> so that heterogeneities form in their composite materials. Very small-scale heterogeneities may be desirable, as in high-impact polystyrene, but more often they render the new material brittle or otherwise unsuitable for its intended use. To design new materials intelligently, it is important to develop a detailed understanding of the phase behaviors of blended polymeric materials as the conditions to which they will be subjected are changed. Various scattering techniques and types of microscopy are useful for studying phase-separating blends,<sup>2</sup> particularly when the heterogeneities are plentiful or large. However, it is also desirable to monitor the formation of guest-component aggregates from the very onset of their phase separation from the host material. Since heterogeneities form more quickly the higher the concentration of the minor component of the blend, the onset of phase separation is best studied at low guest-component concentrations. The sensitivity of the optical method used here allows us to observe the onset of guest copolymer aggregation in the dilute limit, while physical parameters such as blend composition and annealing time and temperature are varied. Because this technique is not complicated by problems of insufficient contrast between the blend

components, it is particularly well suited for the study of multiple-component composites.

The complete process of phase separation of molecularly mixed polymer blends can be observed by monitoring the effects of electronic excitation transfer (EET) on the time-dependent polarization anisotropy decay of fluorescence from chromophores, such as the 2-vinylnaphthalene (2VN) used in these experiments, copolymerized with optically inert monomers, e.g., methyl methacrylate or styrene. The chromophore-bearing guest copolymers are blended in various compositions with an optically inert host material. When the 2VN chromophores are exposed to a short (picosecond time scale) polarized ultraviolet laser pulse, the 2VN molecules with a large projection of their transition dipole along the direction of the optical  $\vec{E}$ -field become optically excited. An excited chromophore can emit a photon, or the excitation can be transferred to a nearby unexcited chromophore through a nonradiative dipole–dipole interaction described by Förster.<sup>3</sup> Fluorescence emitted from the ensemble of initially excited chromophores preserves the initial polarization characteristics established by the excitation field. However, excitations can be transferred to molecules having any transition dipole direction. Chromophores that have become excited via EET produce depolarized fluorescence. Thus, monitoring the time dependence of the fluorescence depolarization provides a method for observing EET. EET is very sensitive to the distances between chromophores. The rate of excitation transfer falls off as  $(R_0/R)^6$ , where  $R$  is the distance between two chromophores and  $R_0$  is the Förster radius of the chromophore, which provides the distance scale in the EET experiment. The probability of transfer decays more quickly the more chromophores are within  $R_0$ . Naphthyl chromophores are used in the experiments presented below ( $R_0 = 13 \text{ \AA}$ ).<sup>4</sup> This technique can reveal the single-chain structure and spatial distribution of polymer chains in a blend on a nanometer

<sup>†</sup> Current address: Center for International Security and Cooperation, Stanford University, Stanford, CA 94305-6165.

<sup>\*</sup> Corresponding author: e-mail fayer@fayerlab.stanford.edu; fax (650) 723-4817.

distance scale. Monte Carlo simulations, in which the likelihood of finding an excitation on an initially excited chromophore at time  $t$  is determined for various chromophore distributions, can be used to analyze the measured decay of the polarization anisotropy of the emitted fluorescence,  $r(t)$ , in terms of the characteristics of the polymer system.<sup>5</sup>

## II. Experimental Methods

**A. Sample Preparation.** Poly[methyl methacrylate-*co*-2-vinylnaphthalene] (PMMA2VN) and poly[methyl methacrylate] (PMMA) are prepared using free-radical polymerization to yield chains of various molecular weights and chromophore compositions, as described previously.<sup>6</sup> (The PMMA is synthesized because commercially available PMMA contains fluorescing species which are difficult to remove.) Specific amounts of the guest polymers (either PMMA2VN alone or with homemade PMMA) and poly[vinyl acetate] (PVAc; Aldrich,  $M_w = 83\,000$ ) are completely dissolved and molecularly mixed<sup>1</sup> in benzene at 5% total polymer weight/benzene volume and promptly freeze-dried. Freeze-dried material is compressed at room temperature to form a pellet. To take "snapshots" of phase-separating blends for analysis, individual pellets are loaded into a Carver press and annealed under vacuum at a specific temperature (77 °C) for a specific time between 20 min and 24 h. Annealed pellets are then pressed at 0.5 metric tons and rapidly quenched below the glass-transition temperature ( $T_g$ ) in dry ice. These samples contain nanoscopic aggregates of guest copolymer that are kinetically trapped in the polymer glass.

In using EET to determine the characteristics of polymer chains, accurate knowledge of the number of chromophores per chain,  $N$ , is essential.  $N$  is determined by spectroscopic measurements of the chromophore-bearing copolymers. The absorption spectrum of a quantitatively prepared copolymer sample is measured, and the extinction coefficient of the chromophore is used to determine the number of chromophores per copolymer molecule. The extinction coefficient is determined using 2-ethylnaphthalene as a model compound. Refined procedures were developed for measuring the extinction coefficient, resulting in a more accurate value for the extinction coefficient than was previously reported.<sup>7</sup> The complete details of the determination of the extinction coefficient appropriate for use in these studies are described in ref 8.

**B. Fluorescence Measurements.** The time-correlated single photon counting technique<sup>9</sup> and our system<sup>10</sup> have been described in detail. The output of an acoustooptically mode-locked Nd:YAG laser is frequency-doubled and used for synchronous pumping of a dye laser tuned to 639 nm (DCM, Exciton). The cavity-dumped dye laser pulses have a repetition rate of 823 kHz and duration of 15 ps and are frequency-doubled to 319.5 nm for absorption by the naphthalene chromophores. The wavelength 319.5 nm is very close to the peak absorption wavelength of naphthalene (320 nm), and it is the "magic wavelength" at which EET is not dispersive, i.e., at which EET does not depend on the sample temperature or excitation wavelength.<sup>11</sup> Dispersive EET and the discovery of the magic wavelength for this system have been discussed and presented in detail by Stein et al.<sup>12,13</sup>

Front-face fluorescence emitted from the sample is passed through a subtractive double monochromator and detected with a microchannel plate (Hamamatsu R1645U-01). The time resolution of the detection system is measured by examining scattered light from the excitation pulse. The instrument response has a full width at half-height of 50 ps. The polarization of the excitation beam is flipped 90° every 20 s with a Pockel's cell, and the intensity of the fluorescence emitted alternately parallel to ( $I_{||}$ ), then perpendicular to ( $I_{\perp}$ ), the excitation beam is measured. The time-dependent anisotropy,  $r(t)$ , of the sample is calculated using

$$r(t) = \frac{I_{||} - I_{\perp}}{I_{||} + 2I_{\perp}} \quad (1)$$

**C. Cloud-Point Measurements.** For cloud-point measurements, a high- $M_w$  PMMA ( $M_w = 50\,000$ ,  $M_w/M_n = 1.31$ ) and a low- $M_w$  PMMA ( $M_w = 16\,500$ ,  $M_w/M_n = 1.47$ ) were each used as purchased from Scientific Polymer Products, Inc., in addition to the copolymers, to make blends with the host PVAc. Blends were prepared in several weight ratios by dissolution of PVAc and PMMA or PMMA2VN in benzene, thorough mixing and lyophilization. Dry blend was loaded into the die cell of a Carver press at room temperature, evacuated, pressed to 0.5 metric tons, and transferred into a calibrated, insulated, temperature-controlled copper cell used to anneal pellets of freeze-dried material from room temperature through the blend's  $T_g$  (~55 °C for these samples) and through the cloud point,  $T_c$ , which was identified as the temperature at which the first hint of opalescence was detected with the aid of a microscope and backscattered illumination. This method of sample preparation was chosen to match that for the samples studied below  $T_g$  as closely as possible. Samples of masses from 20.0 to 191.0 mg and thicknesses of 0.5–1.80 mm were studied to check for the dependence of the observed cloud points on sample thickness; no such dependence was found.

**D. Data Analysis.** The fluorescence anisotropy represents the extent to which the polarization of the fluorescence has persisted after excitation with a short polarized laser pulse. Processes that contribute to the decay of the anisotropy, i.e., to the randomization of the polarization of light emitted by the chromophores, include both intrachain and interchain EET and orientational relaxation of the chromophores on the time scale of the measurement. Since we are interested in only the EET, we must measure and account for the contribution of orientational relaxation to  $r(t)$ . Orientational relaxation is relatively slow compared to the time scale of EET. Orientational relaxation is measured using copolymers with a very low chromophore content, so that intrachain EET is unlikely to occur, in blends with low guest copolymer content, so that contributions from interchain EET are also insignificant. The shape of the  $r(t)$  measured from these blends is reproduced with an empirical analytical function,  $\Phi(t)$ .

The EET contribution to  $r(t)$  is determined by  $\langle G^s(t) \rangle$ , the ensemble-average probability that the initially excited chromophore is still excited at time  $t$ .  $\langle G^s(t) \rangle$  has contributions from excitations that have not left initially excited chromophores, as well as from excitations that have left and returned to initially excited chromophores.  $\langle G^s(t) \rangle$  does not include decay due to the lifetime of the excited state; the denominator of eq 1 removes the lifetime from  $r(t)$ . An analytical theory of  $\langle G^s(t) \rangle$  was developed for EET among chromophores on an ensemble of isolated chains (no interchain transfer).<sup>14</sup> This theory has been shown to be accurate through experiments<sup>15</sup> and comparison to detailed simulations.<sup>5,8</sup> An analytical theory was also developed for interchain EET, i.e., the contribution to  $\langle G^s(t) \rangle$  from excitations that transfer from chromophores on copolymer chains containing the initially excited chromophores to chromophores on other copolymer chains.<sup>16</sup> The initial development of the theoretical method treating interchain transfer was subsequently corrected and tested with Monte Carlo simulations.<sup>5,8</sup> The simulations demonstrated that the corrected analytical theory can be reasonably accurate, but not under all conditions. Because the simulations rely on fewer assumptions than the theory, the probability of finding an excitation on an initially excited chromophore,  $\langle G^s(t) \rangle$ , is determined by simulation for analysis of the data presented here. The improvements in the theoretical methods for analyzing experiments measuring interchain EET<sup>8</sup> and the improved determination of the naphthyl chromophore extinction coefficient<sup>8</sup> should make the data analysis presented below more accurate than that of previous studies,<sup>7,17</sup> although the shortfalls of the previous studies were substantially offsetting.

Because orientational relaxation is slow relative to EET, orientational relaxation and EET are taken to be independent. Then the total decay of the polarization is the product of  $\Phi(t)$  and  $\langle G^s(t) \rangle$ . The product

$$r(t) = \Phi(t)\langle G^s(t) \rangle \quad (2)$$

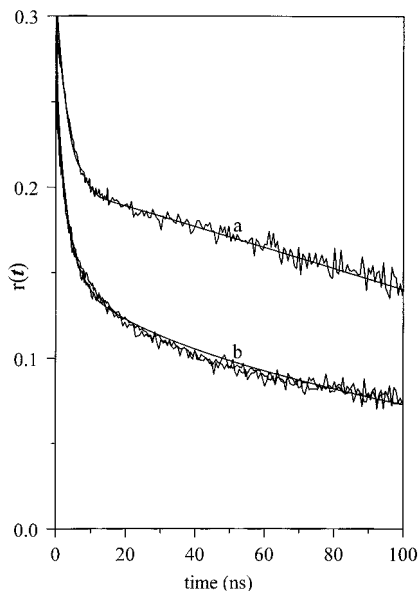


**Figure 1.** Curve a is the fluorescence anisotropy decay,  $r(t)$ , measured from isolated chains of PMMA2VN in PVAc. The low number of chromophores per PMMA2VN chain and the low copolymer concentration ensure that there is no significant EET. The decay is caused by orientational relaxation. The line through the data,  $\Phi(t)$ , is an empirical fit used in subsequent data analysis. Curves b are  $r(t)$ 's measured from blends of 0.05% and 0.1% PMMA2VN ( $M_w = 55\,000$ , 16 chromophores per chain) in PVAc annealed at 77 °C for 20 min. The number of chromophores per chain is sufficiently large for intrachain EET to occur. The fact that the data from blends with 0.05% and 0.1% PMMA2VN give indistinguishable results demonstrates that, for these conditions, there is no appreciable phase separation. The curve through the data is a simulation of EET on isolated chains (no interchain EET). All simulations are multiplied by  $\Phi(t)$  (see text).

is compared with the measured  $r(t)$  obtained from samples in which EET occurs.

### III. Results

**A. Binary Blends.** Figure 1 presents results of fluorescence anisotropy decay measurements of PMMA2VN in PVAc. Curve a is  $r(t)$  in the absence of EET. The blend is composed of 0.05% PMMA2VN with the number of chromophores per chain  $N = 0.2$  (one chromophore for every five copolymer chains,  $M_w = 17\,800$ ) in PVAc. With the very low number of chromophores per chain and the low concentration of PMMA2VN chains in the blend, the chromophores are on average too far apart for any significant EET to occur. The solid line through the data is an empirical fit that is subsequently used for  $\Phi(t)$  in eq 2.

Curves b in Figure 1 are measured from blends of PMMA2VN with  $M_w = 55\,000$  and  $N = 16$  in PVAc. The anisotropy decays are for two blends, one with 0.1% PMMA2VN and another with 0.05% PMMA2VN, both annealed at 77 °C for 20 min. The anisotropy decays recorded from the two blends are virtually identical, indicating that the 0.1% blend prepared in this manner is in the dilute limit, i.e., that individual copolymer chains are isolated from each other and out of range of interchain EET. The solid line through the data is the computed  $r(t)$ , obtained by calculating  $\langle G^2(t) \rangle$  with simulations of EET on isolated chains of this copolymer and multiplying them by  $\Phi(t)$  as per eq 2. As can be seen in the figure, the shape of the calculated decay curve agrees well with that of the data. The fit uses an

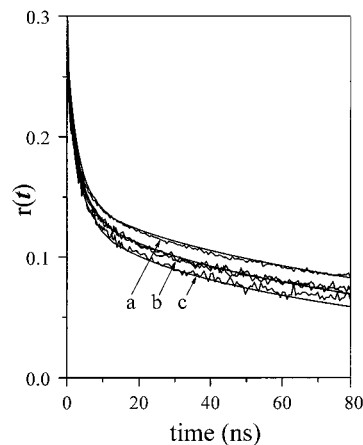


**Figure 2.** Curve a is averaged  $r(t)$  data and the associated simulation (curves b from Figure 1) for isolated chains. Curves b are measured from the guest copolymer in blend samples annealed for 1 and 4 h rather than the 20 min of curve a. The increased rate of decay shows the onset of phase separation; the formation of nanodomains of PMMA2VN in PVAc results in interchain EET. The simulation is for spherical nanodomains containing four PMMA2VN chains (see text). Curve c is for an identical blend sample, annealed for 16 h. Increased phase separation produces a faster decay. The simulation is for spherical nanodomains containing seven PMMA2VN chains (see text).

ensemble-averaged root-mean-square radius of gyration,  $\langle R_g^2 \rangle^{1/2} = 50.5 \text{ \AA}$ . This  $\langle R_g^2 \rangle^{1/2}$  is smaller than the  $\theta$ -condition value of 72 Å because of the unfavorable interactions between PMMA and PVAc which give rise to chain contraction.<sup>15</sup> Within experimental error, the extent of the contraction is the same as that observed previously for a lower molecular weight PMMA2VN copolymer in PVAc.<sup>15</sup>

Figure 2 displays data for blends of PMMA2VN ( $M_w = 55\,000$  and  $N = 16$ ) and PVAc prepared with different annealing times, all annealed at 77 °C. Curve a is the average of the isolated chain data shown in Figure 1. Curves b are data taken from two other samples of the 0.1% blend, annealed for 1 and 4 h. The decays are faster than that measured from the isolated chains. The longer annealing was sufficient for the formation of PMMA2VN aggregates, which are referred to as nanodomains. With several chains close together, interchain EET can occur, and  $\langle G^2(t) \rangle$  decays more quickly than it does for isolated chains. Within experimental error, no difference is observed between the curves for the two annealing times. A sample annealed for 2 h and another sample annealed for 1 h are also indistinguishable from curves b. Curve c displays data measured from a sample annealed for 16 h. The decay is even faster, indicating further aggregation.

The discussion of Figure 2 assumes that the increases in the decay rates of the data with increased annealing times are brought about by the onset of phase separation and the advent of interchain EET in phase-separated nanodomains. There is another possibility that can be tested experimentally. It has been shown above and in previous experiments<sup>15</sup> that PMMA2VN is contracted in PVAc with respect to its size under  $\theta$ -conditions. It is possible that copolymer chains contract more as the annealing time is increased. If further contraction were to occur, the rate of intrachain EET would increase even in the absence of phase separation. As a test, we reduced the number of copolymer chains in the blend by a factor of 2 and repeated the annealing

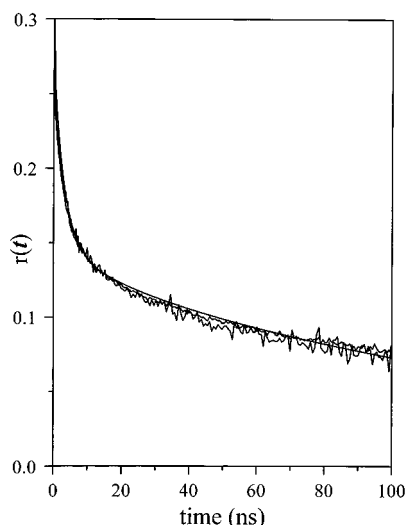


**Figure 3.** The data curve with less noise is the combined  $r(t)$  measured from blends of 0.05% and 0.1% PMMA2VN ( $M_w = 55\,000$ ,  $N = 16$ ) in PVAc annealed at 77 °C for 20 min (Figure 2, curve a), showing intrachain EET. The smooth curve through the data is the corresponding simulation. The data curve with more noise is the  $r(t)$  measured from a blend of 0.05% PMMA2VN in PVAc annealed at 77 °C for 4 h. These results show that, for the reduced concentration of 0.05% copolymer in PVAc, an annealing time of 4 h results neither in further chain contraction nor in the onset of phase separation.

process. Figure 3 shows data from blends of PMMA2VN ( $M_w = 55\,000$ ,  $N = 16$ ) in PVAc in the dilute limit (averaged isolated chain data, reproduced from Figure 2), along with the simulated  $\langle G^2(t) \rangle$  for isolated chains (smooth line), and data from a blend of 0.05% PMMA2VN in PVAc annealed at 77 °C for 4 h. The 0.05% data annealed for 4 h has more noise, because the sample is more dilute and produces less fluorescence. Within experimental error, the data from the more dilute sample annealed for 4 h are the same as the isolated chain data of Figure 2. The  $\langle G^2(t) \rangle$  that fits the data is for intrachain EET only. Thus, for a more dilute sample, the increased annealing time does not increase the rate of EET, indicating that the chains do not undergo additional contraction with increased annealing time. Therefore, it is reasonable to infer that the increased rates of anisotropy decay shown in curves b and c of Figure 2 are due to interchain EET caused by phase separation. Furthermore, the results show that decreasing the concentration by a factor of 2 is sufficient to inhibit nanodomain formation, at least on the 4 h time scale.

Simulations of EET can be used to obtain more quantitative information about the details of phase separation. However, comparisons of data with calculations can only be made within the context of a model of the nature of phase separation, since calculations that fit the data are not necessarily unique. Structures resulting in calculated curves that do not agree with the data can be ruled out. Given an assumption of a particular size and shape of a nanodomain, it is possible to determine how many chains are in the aggregate by comparing simulation and experiment.

Our initial choice for a size and shape with which to describe a nanodomain is made as follows. Since we are not at first focusing on the formation of subdomains within isolated molecules (Figure 3) but seeking instead to model the aggregation of two or more molecules that

begin out of range of interchain EET, we want the volume to be at least as large as that spanned by an "average" single, isolated molecule. Since a single polymer molecule will not fill the space it spans, the domains are assumed to maintain a constant volume while the concentration of copolymer chains in the aggregate increases with annealing time, as in spinodal decomposition.<sup>1</sup> In the calculations, we have considered spherical nanodomains whose radii equal the single copolymer chain  $\langle R_g^2 \rangle^{1/2}$  (50.5 Å), as well as somewhat larger spheres. In the spherical nanodomains, the centers-of-mass of the chains are constrained to lie within a spherical volume. However, significant portions of the chains can reside outside of a spherical nanodomain, since the sphere only limits the locations of the centers-of-mass. Thus, the sphere does not define an abrupt boundary.

In Figure 2, the solid line through curves b is obtained from a simulation of EET including both intrachain and interchain transfer events. The calculation uses spherical nanodomains with radii equal to  $\langle R_g^2 \rangle^{1/2}$  for a single copolymer chain (50.5 Å). The good agreement between the simulation and the data was obtained for four copolymer molecules ( $N_c = 4$ ) in the domain. The solid line through curve c is a simulation for nanodomains of the same size and shape, with  $N_c = 7$ . The polymer density (1.19 g/cm<sup>3</sup> for both guest and host) prevents more than seven copolymer molecules from being completely contained in a spherical volume of radius 50.5 Å. However, in the model of the nanodomains used here, only the centers-of-mass are required to reside within a sphere of radius 50.5 Å. A spherical shell 10 Å wide at the surface of the domain (40.5–50.5 Å) contains 48% of the volume in which the centers of mass may be located. Therefore, the volume in which PMMA2VN chain segments can be located is substantially greater than the spherical volume in which the centers-of-mass are located. In the spherical nanodomain model, the chain-segment density falls off approximately as a Gaussian outside the sphere. Thus, the fit that yields  $N_c = 7$  does not imply that a domain is pure PMMA2VN. A significant fraction of the volume within the sphere can be PVAc, and a large number of PMMA2VN chains will extend outside the sphere and be intermixed with PVAc.

It is also possible to get good fits to the data assuming larger radii for the simulated nanodomains. For example, using spherical nanodomains with  $r = 1.5\langle R_g^2 \rangle^{1/2}$ , a calculated curve with  $N_c = 12$  is obtained that is virtually indistinguishable from that shown through the data in curve c of Figure 2. In Debye's theoretical consideration of the range of interaction between polymer molecules ( $l$ ) and its relationship to the radius of gyration,<sup>18</sup> he assumed that these might be equal and called for experimental investigations to test this hypothesis. In his own subsequent experimental paper,<sup>19</sup> he reported a complex relationship between the two distances and noted "the striking smallness of  $l$  compared with the radius of gyration." A domain much larger than a sphere with  $r = \langle R_g^2 \rangle^{1/2}$  would be inconsistent with Debye's work. For an aggregate to persist, the chains must have significant interaction, and the distance scale,  $l$ , for such an interaction is smaller than the radius of gyration.

In Figure 2, the data indicate a change from the single-chain state (curve a) to that of nanodomains with  $N_c = 4$  (curve b) when the annealing time is increased

from 20 min to 1 h. Within experimental error, the data do not change further for at least an additional 3 h. There is apparently a "stalling" of the increase in the rate of experimental  $r(t)$  decays. This stalling could indicate a slowing of the rate of aggregation or a change in the nature of the aggregation. Possibly, the thermodynamic drive to phase separate is balanced by the kinetic barriers to replacing the PVAc chain segments entangled in a small nanodomain with more PMMA2VN segments. It is also possible that there is an increase in nanodomain volume. As discussed above, curve c in Figure 2 can be fit equally well with seven chains in a volume of radius  $\langle R_g^2 \rangle^{1/2}$  or 12 chains in a radius of  $1.5\langle R_g^2 \rangle^{1/2}$ . If after initial aggregation in the smallest possible nanodomain the nanodomain volume begins to increase, the first few additional chains in the larger volume will have much less impact on the decay than would the addition of these chains into the compact nanodomain. Alternatively, an increase in nanodomain volume and a decrease in the rate of aggregation would also result if the compact nanodomains ceased to grow individually but, through aggregate diffusion, encountered other compact nanodomains and thereby formed larger nanodomains.

We have observed this phenomenon in another series of samples<sup>8</sup> with a copolymer of  $M_w = 25\,300$  and  $N = 36$ . The samples were annealed at  $103\text{ }^\circ\text{C}$ . In that series there is a significant increase in the rate of decay when the annealing time is increased from 20 min to 1 h. There is no apparent change between 1 and 2 h. By the next time point at 8 h, the decay is significantly faster. However, in the series of samples studied as a function of annealing time at  $85\text{ }^\circ\text{C}$  in ref 7, stalling in the phase separation process was not observed.

**B. Ternary Blends.** To gain additional insight into the microscopic details of phase separation, experiments were conducted on ternary blends. The first ternary blend is of 0.1% 55 000  $M_w$  PMMA2VN (in which we observed EET from isolated molecules in curve b of Figure 1), 4.9% synthesized PMMA ( $M_w = 33\,600$ ,  $M_w/M_n = 1.67$ ), and 95% PVAc annealed at  $77\text{ }^\circ\text{C}$  for 4 h. The blend is essentially 5% PMMA and 95% PVAc, but a small fraction of the PMMA is the chromophore-labeled copolymer. In the experiments discussed above, nanodomain formation was observed after 4 h with 0.1% copolymer in PVAc. Therefore, while microscopic phase separation is not observed with 5% PMMA at this temperature after 4 h (see Table 1), there should be substantial nanoscopic phase separation. However, interchain EET should not be observed if the copolymer and the PMMA phase separate together, since the copolymer would form nanodomains consisting predominantly of PMMA chains that are not labeled with chromophores. Thus, the copolymer molecules would be widely separated on average, despite nanodomain formation.

The aim of the ternary blend experiments is to examine the local environment of the copolymer chains. When these chains are isolated in PVAc, they are contracted relative to their size in a  $\theta$ -condition solvent.<sup>15</sup> When the copolymer chains are dilute in PMMA, they have a size that is consistent with being in a  $\theta$ -solvent.<sup>15</sup> The question is, what is the nature of the local environment of a chain in a phase-separated nanodomain? If a copolymer chain finds itself in a region that is essentially pure PMMA, it should expand to the size that was observed in the blends of copolymer with

**Table 1. Cloud-Point Temperatures ( $^\circ\text{C}$ ) for Blends of PMMA or PMMA2VN in PVAc<sup>a</sup>**

vol %	PMMA ( $M_w = 50\,000$ )	PMMA ( $M_w = 16\,500$ )	PMMA2VN ( $M_w = 25\,300$ )
10.0	$\leq 85$	$\leq 77$	
5.0	$\leq 91$	$\leq 79$	$\leq 65$
2.5	$\leq 93$	$\leq 81$	$\leq 65$
0.1			$\leq 75$

<sup>a</sup> The temperature at which a blend of a given composition scatters visible light is called the "cloud point".<sup>1</sup> The cloud-point measurements reported here were used to confirm that the blends used in the excitation transport experiments were annealed at temperatures at which phase separation will occur. The results of cloud-point measurements were found to be extremely sensitive to the initial temperature and rate of heating. Cloud-point curves for PMMA/PVAc blends generated by Qipeng<sup>24</sup> with heating ramps from 2 to  $20\text{ }^\circ\text{C}/\text{min}$  lie well above the equilibrium LCST curve, since a heating ramp of  $2\text{ }^\circ\text{C}$  every 2 h used here gave lower cloud-point temperatures. The cloud-point temperatures given in the table are the observed cloud points and are probably still above the equilibrium critical solution temperature curve. This is indicated by the  $\leq$  signs in the table. Measuring the critical solution temperatures may not be kinetically possible, since the polymers become drastically less mobile at lower temperatures near the blends'  $T_g$ 's. This is the reason for the apparent discrepancy in which higher molecular weight polymer has a higher observed cloud-point temperature. For a more detailed discussion of these measurements, see ref 8.

PMMA; i.e., it should expand to its  $\theta$ -condition size. If the nanodomain contains a substantial amount of PVAc, it should remain contracted.

Data from the first ternary blend sample is shown in Figure 4A along with data for the isolated chains in PVAc (contracted, but no interchain EET), curve b of Figure 2. Within experimental uncertainty, the curves are identical. These data also match the simulation of EET on single chains in PVAc (smooth line) even though the blend is 5% PMMA and has been annealed for 4 h. Thus, when PMMA is present, EET between different molecules of PMMA2VN is not observed, but neither is chain expansion. The fact that the PMMA2VN chains do not expand indicates that they are still in substantial contact with PVAc. The PMMA2VN is not in regions that are essentially pure PMMA. The results in section III.A indicate that even for the smallest possible nanodomains with  $r = \langle R_g^2 \rangle^{1/2}$  there is a significant number of PVAc chains intermixed with the copolymer at the early stages of phase separation. If the size of the domains is larger, e.g.,  $r = 1.5\langle R_g^2 \rangle^{1/2}$ , there will be even more PVAc in the nanodomains. These results indicate that the first ternary blend has nanoscopic phase separation that involves a significant intermixing of PVAc and PMMA chains.

A second ternary blend was prepared consisting of 0.1% 55 000  $M_w$  PMMA2VN, 18.9% PMMA, and 81% PVAc (19% PMMA-like guests). This blend was annealed at  $77\text{ }^\circ\text{C}$  for 20 min. The annealing time was reduced to prevent macroscopic phase separation; under these conditions, the sample did not have time to reach its cloud point. Data from this sample are shown in Figure 4B, curve a, along with a simulated curve. Curves b are from isolated, contracted chains (reproduced from Figure 4A for easy comparison). The 19% ternary blend data clearly decay more slowly than data from the contracted form of the copolymer. The smooth line presented with curve a is a simulation of  $\langle G^s(t) \rangle$  for the isolated copolymer in  $\theta$ -conditions (no interchain EET, no contraction). The agreement is quite reasonable. The results indicate that in the second ternary

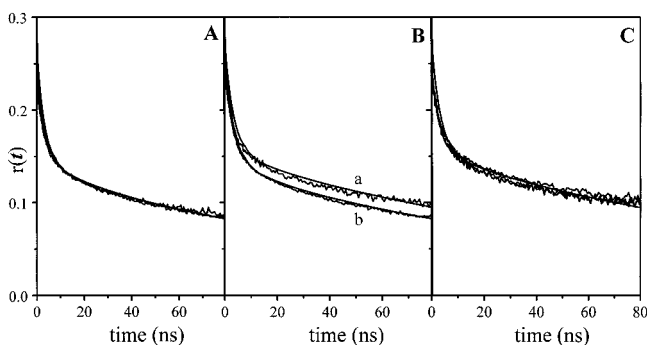


**Figure 4.** (A)  $r(t)$  measured from a binary blend of 0.1% PMMA2VN ( $M_w = 55\,000$ ,  $N = 16$ ) in PVAc annealed at 77 °C for 20 min and from a ternary blend of 0.1% PMMA2VN, 4.9% PMMA ( $M_w = 33\,600$ ), and PVAc annealed for 4 h at 77 °C. Within experimental error, the curves are identical. Also shown (smooth curve) is a simulation for isolated, contracted copolymer chains. Although phase separation occurs, the copolymer  $r(t)$  in the ternary blend shows no interchain EET, and the intrachain EET is characteristic of contracted copolymer chains, i.e., those in contact with PVAc. (B) Curve a is  $r(t)$  measured from a ternary blend of 0.1% PMMA2VN, 18.9% PMMA ( $M_w = 33\,600$ ), and PVAc annealed for 20 min at 77 °C and a simulation of intrachain EET for the copolymer in  $\theta$ -conditions, i.e., in pure PMMA. The  $r(t)$  shows that the copolymer chains have expanded, indicating that they are in environments of essentially pure PMMA. For comparison, curve b shows data and a simulation for intrachain EET on contracted copolymer chains, i.e., on copolymer molecules interacting with PVAc. (C) The data curve a from (B) (the 19% ternary blend data) is shown with data from two samples of a binary blend of 0.1% PMMA2VN in PMMA, the  $\theta$ -condition host, annealed for 20 min and 16 h. Also shown is the  $\theta$ -condition simulation. All of the data curves are the same, within experimental error. This comparison demonstrates that the copolymer in the 19% ternary blend has a structure consistent with its being in an essentially pure PMMA environment.

blend with 19% PMMA the copolymer PMMA2VN finds itself in an essentially pure PMMA environment.

Figure 4C supports this interpretation of the nature of the 19% PMMA ternary blend. The data curve a from Figure 4B (the 19% ternary blend data) is shown with data from two samples of a binary blend of 0.1% PMMA2VN in PMMA, the  $\theta$ -condition host, annealed for 20 min and 16 h, respectively. Also shown is the simulation of intrachain transfer under  $\theta$ -conditions. All of the data curves are the same within experimental error. This comparison confirms that the copolymer in the 19%, 20 min annealing time ternary blend has a structure consistent with its being in a pure PMMA environment.

We have demonstrated that PMMA2VN aggregates to form nanodomains in PVAc (Figure 2) and that, in ternary blends with PMMA, the copolymer forms domains with PMMA as phase separation begins but still has substantial interaction with PVAc (Figure 4A). Furthermore, the results show that when phase separation proceeds, the copolymer expands as it would in an essentially pure PMMA environment (Figure 4B,C). However, the observed cloud points of PMMA2VN/PVAc blends at much lower temperatures than those of analogous PMMA/PVAc blends (see Table 1) indicate that the phase behavior of PMMA2VN in PVAc is not identical to that of PMMA in PVAc. The stacking affinity of these chromophore side groups in polymer chains<sup>20</sup> may account for this observation. There is some evidence in the following ternary experiments that, given enough time, PMMA2VN segregates from PMMA after

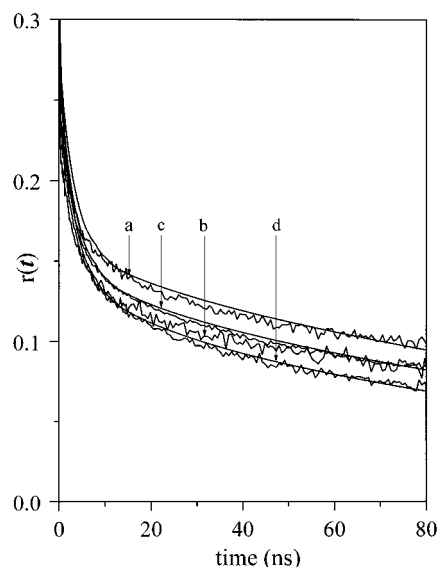


**Figure 5.** Curve a is  $r(t)$  measured from a ternary blend of 0.1% PMMA2VN, 18.9% PMMA, and PVAc annealed for 20 min at 77 °C, shown with the simulation for the copolymer in PMMA ( $\theta$ -condition). Curve b is  $r(t)$  measured from a ternary blend of 0.1% PMMA2VN, 18.9% PMMA, and PVAc annealed for 4 h at 77 °C. Curves c are  $r(t)$  data and simulation for the binary blend of the copolymer in PVAc annealed for 20 min at 77 °C. Curve d is  $r(t)$  measured from the binary blend of the copolymer in PVAc annealed for 4 h at 77 °C, shown with the simulation of EET in a nanodomain with four chains. Curves c and d are curves a and b of Figure 2, reproduced here for comparison. Curve b demonstrates that the increased annealing time of the 19% blend has resulted in aggregation of the copolymer chains within the PMMA domains. The shape of the  $r(t)$  curve shows that the aggregate is not a spherical nanodomain.

the initial formation of essentially pure copolymer/PMMA domains in PVAc.

Curve b of Figure 5 displays data from a 19% ternary blend annealed at 77 °C for 4 h. Curve a is data for the  $\theta$ -condition chain along with the corresponding calculated curve. Curve c is data from the contracted single chain along with the corresponding calculated curve. Curves c and b become coincident at long times but have decidedly different shapes at short times. Curve d is data from the nanophase-separated binary blend (Figure 2, curve b) annealed for 4 h and the associated calculated curve. While the 19% ternary blend annealed for 20 min gave a  $\theta$ -condition-like decay (curve a), the 19% ternary blend annealed for 4 h yields a much faster decay (curve b). However, this decay is distinct from both the contracted chain decay (curve c) and the nanophase-separated decay from the binary blend (curve d). Extending the annealing time to 4 h in the 19% blend apparently changes the copolymer from isolated  $\theta$ -condition chains embedded in PMMA domains to something else.

One possibility that would explain the fast decay of curve b is that, after phase separating with PMMA, the copolymer is extruded from the PMMA domains to their surfaces. Extrusion would bring the copolymer into contact with PVAc, which could result in chain contraction. However, the cloud point measurements shown in Table 1 demonstrate that the copolymer has a greater tendency to phase separate from PVAc than from PMMA. The experiments presented above indicate that the copolymer in the ternary blends phase separates along with PMMA, at least initially. Thus, it seems

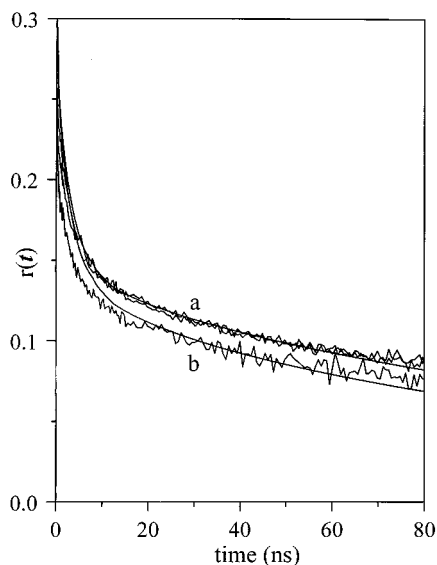


**Figure 6.** Curves a are  $r(t)$  measured from ternary blends of 0.1% PMMA2VN, 4.9% PMMA, and PVAc annealed for 20 min and 4 h at 77 °C. Also shown (smooth curve) is a simulation for isolated, contracted copolymer chains. Curves a are from Figure 4A for comparison with curve b, which is  $r(t)$  measured from the ternary blend of 0.1% PMMA2VN, 4.9% PMMA, and PVAc annealed for 16 h at 77 °C, shown with the simulation of EET in a nanodomain containing four copolymer chains. The sample has passed through the cloud point. Curve b demonstrates that increased annealing time of the 5% blend has resulted in aggregation of the copolymer chains within the PMMA domains. The shape of the  $r(t)$  curve, which does not match the simulation, shows that the aggregate is not a spherical nanodomain.

unlikely that after phase separation the copolymer would find a PVAc environment more favorable than a PMMA environment.

The faster  $r(t)$  may result from aggregation of PMMA2VN within PMMA domains. The change from curve a to curve b produced by increased annealing suggests that PMMA2VN will form its own phase in this ternary system, even when present at very low concentration (0.1%). The unique shape of curve b indicates that the structure of the copolymer aggregate in PMMA cannot be modeled with a spherical nanodomain.

Figure 6 shows anisotropy decays from samples of the ternary blend with 0.1% copolymer, 4.9% PMMA in PVAc. Curves a (as in Figure 4A) are annealed for 20 min and 4 h. Also shown is the simulation of intrachain EET. Curves a are shown for comparison with curve b. Curve b is data from a sample of this same ternary blend, which has been annealed for 16 h. This sample has passed through the cloud point. As in Figure 5, curve b, the increased annealing time has resulted in a more quickly decaying  $r(t)$ . Also shown is the best agreement that can be achieved using simulations of EET in spherical nanodomains. Such simulations matched the shape of data from binary blends of PMMA2VN in PVAc reasonably well (Figure 2). It is clear that the spherical nanodomain simulation does not reproduce the shape of the decay from this ternary blend nearly as well. In particular, the data is badly missed at short times and tails up at long times. The fits to other curves, for both isolated chains and nanodomains, show some discrepancy at long times. The source of this is unknown and may be an experimental artifact. However, curves b in both Figures 5 and 6 clearly have different forms than either the isolated chain curves or

the spherical nanodomain curves. One possibility is that network-like filaments of PMMA2VN are condensing out of the phase-separating blends, forming aerogel-like structures such as those described in ref 23, perhaps after an initial stage of spherical droplet-like nanodomain formation.<sup>1</sup>

#### IV. Concluding Remarks

Electronic excitation transport has been used to study phase separation in binary and ternary blends. The results demonstrate that it is possible to examine processes associated with the phase separation of a polymer composite from the onset of phase separation through the cloud point. This can be accomplished by freezing the structure of a phase-separating blend (rapidly dropping the temperature below the glass transition) and measuring the rate of EET in the resulting kinetically trapped material. Another approach is to measure EET from melts as phase separation is occurring.<sup>22</sup> The comparisons of data and Monte Carlo simulations reported above show that simulations are useful for analyzing data from phase-separating polymer composites. The observations are consistent with a model in which PMMA2VN forms spherical nanodomains in binary blends with PVAc at the onset of phase separation, although as discussed in connection with the data analysis of Figure 2, it is not possible to determine uniquely the size of a nanodomain and the number of chains in it.

In ternary blends of PMMA2VN, PMMA, and PVAc, the copolymer partitions into nanodomains along with PMMA. In small domains the copolymer still has significant contact with PVAc, and the copolymer chains are contracted as they are in PVAc alone. When there is more extensive phase separation, the copolymer expands to its  $\theta$ -condition size, indicating that it is in an essentially pure PMMA environment. However, if the extensively phase-separated ternary blend is annealed for a long time, the data suggest that the copolymer segregates from the PMMA in a form that is not well described as a spherical domain.

The EET approach to the study of phase behaviors in polymer composites should be applicable to a wide variety of systems. However, it is necessary to be able to synthesize a copolymer containing a small number of chromophores that are to be used as the EET probe of the phase-separation process. Studies of the compatible polymer composite, PS/PVME, have begun.<sup>23</sup> It may be possible to use chromophores with different  $R_0$ 's to analyze the structures of the same polymer systems on various distance scales. The effects of pressure on phase behavior are readily accessible to the "snapshot" method, simply by varying the pressure during annealing in the Carver press.<sup>8</sup> While in many respects EET experiments are not as quantitative as methods such as neutron scattering, they can be used to investigate processes that are not amenable to study by other techniques. The sensitivity of fluorescence detection for low-concentration species allows the study of blends in the dilute limit, and the absence of contrast problems permits the study of multicomponent blends.

**Acknowledgment.** We acknowledge the support of the Department of Energy, Office of Basic Energy Sciences (Grant DE-FG03-84ER13251). D.M.H. thanks the Soroptimists of the Sierra Pacific Region for a Dissertation Year Fellowship.

## References and Notes

- (1) Olabisi, O.; Robeson, L. M.; Shaw, M. T. *Polymer-Polymer Miscibility*; Academic Press: New York, 1979.
- (2) See for example: *Neutron, X-ray and Light Scattering: Introduction to an Investigative Tool for Colloidal and Polymeric Systems*; Lindner, P., Zemb, Th., Eds.; Elsevier: Amsterdam, New York, 1991. Iizuka, N.; Bodycomb, J.; Hasegawa, H.; Hashimoto, T. *Macromolecules* **1998**, *31*, 7256. Laurer, J. H.; Hajduk, D. A.; Dreckötter, S.; Smith, S. D.; Spontak, R. J. *Macromolecules* **1998**, *31*, 7546. Simmons, S.; Thomas, E. L. *Polymer* **1998**, *39*, 5587.
- (3) Förster, Th. *Ann. Phys (Leipzig)* **1948**, *2*, 55; *Z. Naturforsch. A* **1949**, *4*, 321.
- (4) Ediger, M. D.; Domingue, R. P.; Peterson, K. A.; Fayer, M. D. *Macromolecules* **1985**, *18*, 1182.
- (5) Hussey, D. M.; Matzinger, S.; Fayer, M. D. *J. Chem. Phys.* **1998**, *109*, 8708.
- (6) Peterson, K. A.; Zimmt, M. B.; Linse, S.; Domingue, R. P.; Fayer, M. D. *Macromolecules* **1987**, *20*, 168.
- (7) Marcus, A. H.; Hussey, D. M.; Diachun, N. A.; Fayer, M. D. *J. Chem. Phys.* **1995**, *103*, 8189.
- (8) Hussey, D. M. Theoretical Analysis, Simulations, and Experimental Investigations of Electronic Excitation Transport in Polymer Composites. Ph.D. Thesis, Stanford University, 1998.
- (9) O'Connor, D. V.; Phillips, D. *Time-Correlated Single Photon Counting*; Academic Press: London, 1984.
- (10) Stein, A. D.; Peterson, K. A.; Fayer, M. D. *J. Chem. Phys.* **1990**, *92*, 5622.
- (11) Fayer, M. D. In *Laser Optics of Condensed Matter*; Plenum Press: New York, 1991; Vol. 2.
- (12) Stein, A. D.; Peterson, K. A.; Fayer, M. D. *Chem. Phys. Lett.* **1989**, *161*, 16.
- (13) Stein, A. D.; Peterson, K. A.; Fayer, M. D. *J. Chem. Phys.* **1990**, *92*, 5622.
- (14) Peterson, K. A.; Fayer, M. D. *J. Chem. Phys.* **1986**, *85*, 4702.
- (15) Peterson, K. A.; Stein, A. D.; Fayer, M. D. *Macromolecules* **1990**, *23*, 111.
- (16) Marcus, A. H.; Fayer, M. D. *J. Chem. Phys.* **1991**, *94*, 5622.
- (17) Marcus, A. H.; Diachun, N. A.; Fayer, M. D. *Macromolecules* **1993**, *26*, 3041. Marcus, A. H.; Fayer, M. D.; Curro, J. G. *J. Chem. Phys.* **1994**, *100*, 9156. Marcus, A. H.; Diachun, N. A.; Fayer, M. D. *J. Phys. Chem.* **1992**, *96*, 8930. Finger, K. U.; Marcus, A. H.; Fayer, M. D. *J. Chem. Phys.* **1994**, *100*, 271.
- (18) Debye, P. *J. Chem. Phys.* **1959**, *31*, 680.
- (19) Debye, P.; Chu, B.; Woermann, D. *J. Chem. Phys.* **1962**, *36*, 1803.
- (20) Vala, Jr., M. T.; Haebig, J.; Rice, S. A. *J. Chem. Phys.* **1965**, *43*, 886. Fox, R. B.; Price, T. R.; Cozzens, R. F.; McDonald, J. R. *J. Chem. Phys.* **1972**, *57*, 534. Irie, M.; Kamijo, T.; Aikawa, M.; Takemura, T.; Hayashi, K.; Baba, H. *J. Phys. Chem.* **1977**, *81*, 1571.
- (21) Hench, L. L., West, J. K., Eds. *Chemical Processing of Advanced Materials*; J. Wiley & Sons: New York, 1992.
- (22) Hussey, D. M.; Keller, L.; Fayer, M. D. *SPIE Proc.: Adv. Fluoresc. Sensing Technol. III* **1997**, *2980*, 446.
- (23) Diachun, N. A.; Hussey, D. M.; Fayer, M. D. *J. Phys. Chem.* **1998**, *102*, 7112.
- (24) Qipeng, G. *Polym. Commun.* **1990**, *31*, 712.

MA9904114